Polar magnetization unveiled by polarized neutron diffraction

S. W. Lovesey

Published version information

Citation: SW Lovesey. Polar magnetization unveiled by polarized neutron diffraction. Phys Rev B 106, no. 6 (2022): 064415

DOI: 10.1103/PhysRevB.106.064415

Polar magnetization unveiled by polarized neutron diffraction

S. W. Lovesey
ISIS Facility, STFC, Didcot, Oxfordshire OX11 0QX, United Kingdom
and Diamond Light Source Ltd, Didcot, Oxfordshire OX11 0DE, United Kingdom

(Received 12 April 2022; revised 30 June 2022; accepted 25 July 2022; published 11 August 2022)

Polar magnetism is compulsory when magnetic ions occupy sites that are not centers of inversion symmetry. Such magnetism is known to be visible in neutron diffraction, the technique of choice for magnetic structure determinations. Experiments in which the diffracted neutron polarization is analyzed are not a novelty. Symmetry-informed simulations of polarized neutron diffraction (PND) amplitudes for room-temperature hematite (α-Fe_2O_3) illustrate the wealth of information on offer in future experiments. Two magnetic motifs, distinguished by the orientation of their bulk ferromagnetism and delineated by magnetic space groups $C2/c$ and $C2'/c'$, are current front-runners for room-temperature hematite. Both motifs are endowed with polar magnetism and iron Dirac (magnetoelectric) multipoles. The technique of resonant x-ray Bragg diffraction has previously been used to expose Dirac multipoles in room-temperature hematite. For unspecified reasons, the authors of a recent PND study of hamatite do not mention the compulsory polar magnetism, the published observation of Dirac multipoles, or the direct confirmation of neutron scattering by Dirac multipoles [H. Thoma *et al.*, Phys. Rev. X **11**, 011060 (2021).]. The authors omission of polar magnetism in fits to their extensive neutron diffraction patterns calls for a reassessment of the claim to have determined the absolute direction of the Dzyaloshinskii-Moriya interaction.

DOI: 10.1103/PhysRevB.106.064415

I. INTRODUCTION

The well-established technique of polarized neutron diffraction (PND) is a very sensitive probe of magnetic order applicable to a class of antiferromagnets, e.g., MnF_2 and NiF_2 with Mn and Ni ions using centrosymmetric sites in a rutile-type crystal structure [1,2]. Indeed, for the technique to be useful, magnetic order must not break translation symmetry in a centrosymmetric crystal with anti-inversion absent in the magnetic crystal class. Specifically, PND is not suitable for studies of magnetic order in magnetoelectric materials.

The room-temperature magnetic structure of hematite (α-Fe_2O_3), so-called phase II [3,4], meets the three material requirements for a PND investigation. The Greek philosopher Theophrastus is said to mention ichorlike hematite at around 315 B.C., with later work by the father of magnetism, William Gilbert of Colchester, in the 16th century. Its magnetic behavior was studied in the early 20th century by Honda and Soné (1914). Notably, Dzyaloshinskii in 1958 defined hematite as a canted antiferromagnet possessed of the prototype Dzyaloshinskii-Moriya (DM) interaction [5,6]. Iron ions in hematite are believed to occupy sites devoid of symmetry. In which case spatial inversion is absent in site symmetry, and by dint of the "totalitarian principle" of symmetry, attributed to Murray Gell-Mann [7], polar magnetism is compulsory. Whereupon, magnetic polar multipoles, called Dirac multipoles, exist alongside magnetic axial electronic multipoles associated with conventional magnetism. The Dirac dipole is also known as an anapole or toroidal dipole, depicted in Fig. 1. Resonant x-ray Bragg diffraction has exposed Dirac multipoles in several materials, including hematite phase II [8,9], and a direct observation of anapoles by neutron diffraction exploited polarization analysis [10].

We have calculated PND signals for hematite phase II including Dirac multipoles, and a spin-flip ratio that measures the magnetic content of a Bragg spot. The magnetic structure of α-Fe_2O_3 remains unsettled, and our calculations are made with two favored candidates. Bulk ferromagnetism is confined to the basal plane in one candidate (space group $C2/c$ [11,12]), while it is confined to a plane normal to it in a second candidate (space group $C2'/c'$ BNS [11]).

II. CRYSTAL AND MAGNETIC STRUCTURES

The chemical structure of hematite is hexagonal $R\bar{3}c$ (No. 167), with ferric (Fe^{3+}, $3d^5$) ions in sites $12c$ with coordinates (0, 0, 0.1447), and symmetry 3. Oxygen ions (O^{2-}) occupy sites $18e$.

Magnetic structures use monoclinic $C2/c$ (No. 15.85, magnetic crystal class $2/m$ or C_{2h}) or $C2'/c'$ (No. 15.89, $2'/m'$) with Fe ions in sites $8f$ devoid of symmetry. The $C2/c$ structure was proposed by Przeniosło *et al.* [12], but no consensus has been reached. Both structures possess a center of inversion symmetry, and permitted terms in the thermodynamic potential include H and HEE, where H and E are magnetic and electric fields. They have different piezomagnetic properties, however, with eight ($C2/c$) and ten ($C2'/c'$) elements in the corresponding tensor. Local monoclinic axes and the parent structure are related by a basis $= \{(-2, -1, 0),\ (0, -1, 0),\ (2/3, 1/3, 1/3)\}$ with

origin $(1/6, -1/3, 1/6)$. Motifs of magnetic dipole moments are (m_x, m_y, m_z), $(-m_x, m_y, -m_z)$, (m_x, m_y, m_z), $(-m_x, m_y, -m_z)$ in $C2/c$, and (m_x, m_y, m_z), $(m_x, -m_y, m_z)$, (m_x, m_y, m_z), $(m_x, -m_y, m_z)$ in $C2'/c'$.

Monoclinic Miller indices are $h = -(2H_o + K_o)$, $k = -K_o$ and $l = (1/3)(2H_o + K_o + L_o)$ where (H_o, K_o, L_o) are integer Miller indices for $R\bar{3}c$. Diffraction by Fe nuclei is forbidden with L_o odd. Axes for the hexagonal structure are $\mathbf{a}_h = a(1, 0, 0)$, $\mathbf{b}_h = (a/2)(-1, \sqrt{3}, 0)$, and $\mathbf{c}_h = c(0, 0, 1)$ (lattice parameters $a \approx 5.035$ Å, $c \approx 13.758$ Å [13]). Iron multipoles are referred to as orthogonal axes $(\boldsymbol{\xi}, \boldsymbol{\eta}, \boldsymbol{\zeta})$ based on $(\mathbf{a}_m^*, \mathbf{b}_m, \mathbf{c}_m)$, e.g., $\boldsymbol{\eta} = \mathbf{b}_m/|\mathbf{b}_m|$. Here, $\mathbf{a}_m = -\sqrt{3}(a/2)(\sqrt{3}, 1, 0)$, $\mathbf{b}_m = -\mathbf{b}_h$, and $\mathbf{c}_m = (1/3)(-\mathbf{a}_m + \mathbf{c}_h) = (c/2)(t, t/\sqrt{3}, 2/3)$, with $t = (a/c)$ and an obtuse angle $\beta_o \approx 122.39^o$ between $\mathbf{a}_m$ and $\mathbf{c}_m$. The monoclinic cell volume $= a^2c/\sqrt{3}$, which is 2/3 of the hexagonal cell volume. Note that $\mathbf{a}_m$ and $\mathbf{b}_h = -\mathbf{b}_m$ are orthogonal vectors in the plane normal to $\mathbf{c}_h$. A monoclinic reciprocal-lattice vector $\mathbf{a}_m^* \propto (\sqrt{3}, 1, -t2\sqrt{3})$ is orthogonal to $\mathbf{b}_m$ and $\mathbf{c}_m$. In $C2'/c'$ the antiferromagnetic motif of axial dipole moments uses $\mathbf{b}_h$ while the ferrocomponent is in the plane spanned by $\mathbf{a}_m$ and $\mathbf{c}_m$.

Electronic properties of iron ions are encapsulated in spherical multipoles present in the ground state. To begin with, the time-average, or expectation value, denoted by angular brackets $\langle \cdots \rangle$, of spin $\mathbf{S}$ and orbital angular momentum $\mathbf{L}$ form the conventional magnetic dipole moment $\langle 2\mathbf{S} + \mathbf{L} \rangle$ of an Fe ion. Cartesian (x, y, z) and spherical components n_q of a dipole $\mathbf{n}$ are related by $x = (n_{-1} - n_{+1})/\sqrt{2}$, $y = i(n_{-1} + n_{+1})/\sqrt{2}$, and $z = n_0$. More generally, Fe spherical multipoles $\langle U_Q^K \rangle$ of integer rank K possess projections Q in the interval $-K \leqslant Q \leqslant K$, with $K = 1$ for a dipole [14,15]. While all required multipoles are magnetic, i.e., time-odd, we need axial (parity-even) and polar (parity-odd) varieties.

III. BRAGG DIFFRACTION

We adopt a unit-cell structure factor for Bragg diffraction,

$$\Psi_Q^K = \left[\exp(i\kappa \cdot \mathbf{r}) \left\langle U_Q^K \right\rangle_{\mathbf{r}}\right], \tag{1}$$

where the reflection vector κ is defined by (h, k, l), and the implied sum in Ψ_Q^K is over all Fe sites $\mathbf{r}$ in a unit cell. Environments at the four Fe sites in the monoclinic cell are related by the operations of inversion and twofold rotation about the unique axis η. The reflection condition $h + k$ even holds for a C-face centered cell. One finds [11]

$$\begin{aligned}
\Psi_Q^K(C2/c \text{ and } C2'/c') &= [1 + (-1)^{h+k}] \\
&\quad \times \left[\alpha \left\langle U_Q^K \right\rangle + (-1)^Q \beta \left\langle U_{-Q}^K \right\rangle\right], \\
\alpha &= \{\exp(i\varphi) + \sigma_\pi \exp(-i\varphi)\}, \\
\beta &= \Phi(-1)^{K+l}\{\exp(i\varphi') + \sigma_\pi \exp(-i\varphi')\}.
\end{aligned} \tag{2}$$

Here, $\Phi = +1(-1)$ for $C2/c$ ($C2'/c'$) and $\sigma_\pi = +1$ (-1) for parity-even (parity-odd, Dirac) multipoles. Angles in α and β are $\varphi = 2\pi(xh + yk + zl)$ and $\varphi' = 2\pi(-xh + yk - zl)$, with fractional coordinates $y = 1/4$, $x \approx 0.395$, and $z \approx 0.934$. Influential selection rules stem from identities $[\sin(\varphi) - \sin(\varphi')] = [\cos(\varphi) + \cos(\varphi')] = 0$ for k odd. For $[\sin(\varphi) - \sin(\varphi')]$ and $[\cos(\varphi) + \cos(\varphi')]$ are proportional to $\cos(\pi k/2)$, while $[\sin(\varphi) + \sin(\varphi')]$ and $[\cos(\varphi) - \cos(\varphi')]$ are proportional to $\sin(\pi k/2)$.

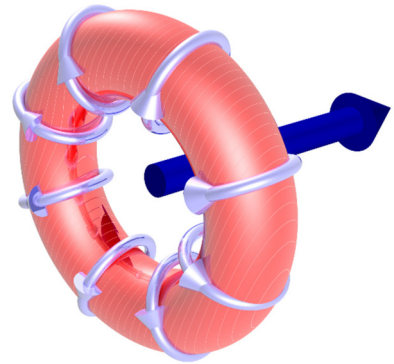

FIG. 1. Depiction of an orbital anapole (toroidal dipole); author V. Scagnoli.

It is convenient in calculations of a neutron scattering amplitude $\langle \mathbf{Q} \rangle$ to express it in terms of quantities that are even and odd functions of projections [15]. From Eq. (2) we find

$$A_Q^K,\ B_Q^K = (1/2)\,[1 + (-1)^{h+k}]\,[\alpha \pm (-1)^Q \beta]\left[\left\langle U_Q^K \right\rangle \pm \left\langle U_{-Q}^K \right\rangle\right]. \tag{3}$$

The upper (lower) sign belongs to $A_Q^K(B_Q^K)$. Notably, β depends on parity σ_π, multipole rank K, Miller index l, and motif signature $\Phi = \pm 1$, together with the angle φ', while α depends on σ_π and the angle φ alone. In particular, Cartesian components of a dipole are derived from $A_0^1 \propto [\alpha + \beta]\langle U_\zeta^1 \rangle$, $A_1^1 \propto i[\alpha - \beta]\langle U_\eta^1 \rangle$, and $B_1^1 \propto [\alpha + \beta]\langle U_\xi^1 \rangle$.

To examine bulk properties, set $h = k = l = 0$ that results in $\varphi = \varphi' = 0$. For these conditions, Dirac multipoles obey Ψ_Q^K ($C2/c$ and $C2'/c'$) $= 0$. Axial multipoles $\langle \mathbf{T}^K \rangle$, with $\sigma_\pi = +1$, in the two monoclinic structures are different. Setting $K = 1$ in Eq. (2) it follows that Ψ_0^1 $(C2/c) = 0$ together with $\Psi_{+1}^1(C2/c) \propto \langle T_\eta^1 \rangle$, meaning the bulk ferromagnetic moment lies along $\mathbf{b}_h$. Turning to $\Psi_Q^1(C2'/c')$, one finds $\Psi_0^1(C2'/c') \propto \langle T_\zeta^1 \rangle$ and $\Psi_{+1}^1(C2'/c') \propto \langle T_\xi^1 \rangle$, so the ferromagnetic moment lies in the plane defined by $\mathbf{a}_m$ and $\mathbf{c}_m$ that is normal to $\mathbf{b}_h$.

Most importantly, magnetic multipoles in neutron diffraction depend on the magnitude of the reflection vector, κ. Figure 2 shows radial integrals, also known as atomic form factors, which occur in dipoles. Dipoles $\langle \mathbf{T}^1 \rangle$ depend on standard radial integrals $\langle j_0(\kappa) \rangle$ and $\langle j_2(\kappa) \rangle$ displayed in Fig. 2, with $\langle j_0(0) \rangle = 1$ and $\langle j_2(0) \rangle = 0$. A useful result is [15]

$$\left\langle \mathbf{T}^1 \right\rangle \approx (1/3)\,[2\langle \mathbf{S} \rangle \langle j_0(\kappa) \rangle + \langle \mathbf{L} \rangle\,(\langle j_0(\kappa) \rangle + \langle j_2(\kappa) \rangle)]. \tag{4}$$

The coefficient of $\langle \mathbf{L} \rangle$ is approximate, while $\langle \mathbf{T}^1 \rangle = (1/3)\langle 2\mathbf{S} + \mathbf{L} \rangle$ for $\kappa \to 0$ is an exact result.

The magnetic polar dipole $\langle \mathbf{d} \rangle$ depends on three radial integrals displayed in Fig. 2. We use [15]

$$\langle \mathbf{d} \rangle = (1/2)\,[i(g_1)\langle \mathbf{n} \rangle + 3(h_1)\langle \mathbf{S} \times \mathbf{n} \rangle - (j_0)\langle \boldsymbol{\Omega} \rangle]. \tag{5}$$

Radial integrals (g_1) and (j_0) diverge in the forward direction of scattering $(\kappa \to 0)$, and (h_1) is also the κ dependence of the polar spin quadrupole observed in neutron diffraction from high-T_c compounds Hg1201 and YBCO [17,18]. Dipoles

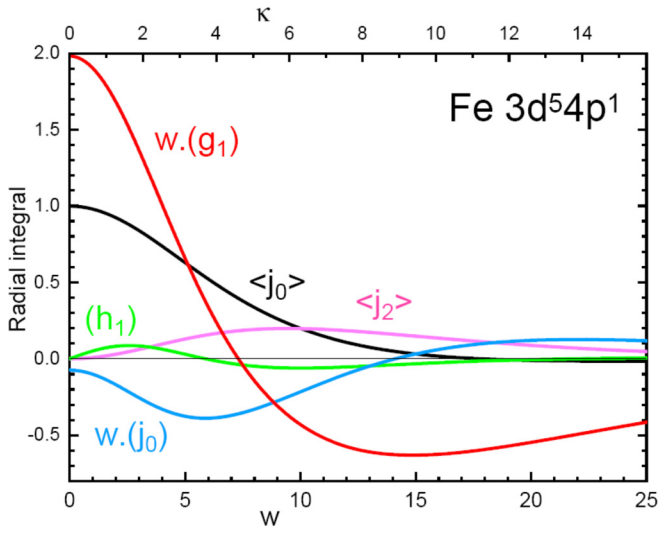

FIG. 2. Radial integrals for the ferric ion $Fe^{3+}(3d^5)$ displayed as a function of the magnitude of the reflection vector $\kappa = 4\pi s$ with $s = \sin(\theta)/\lambda(\text{Å}^{-1})$, Bragg angle θ, and neutron wavelength λ. Also, $w = 3a_o\kappa$ where a_o is the Bohr radius. Blue and purple lines depict standard radial integrals $\langle j_0(\kappa)\rangle$ and $\langle j_2(\kappa)\rangle$ that occur in the axial dipole Eq. (4). Red, green, and blue curves are the radial integrals in the polar dipole Eq. (5). Two integrals (g_1) and (j_0) diverge in the forward direction of scattering and $w(g_1)$ and $w(j_0)$ are displayed. Calculations using Cowan's atomic code [16] and figure by G. van der Laan.

$\langle \mathbf{S}\times\mathbf{n}\rangle$ and $\langle\mathbf{\Omega}\rangle = [\langle\mathbf{L}\times\mathbf{n}\rangle - \langle\mathbf{n}\times\mathbf{L}\rangle]$ are spin and orbital anapoles, and the latter (toroidal dipole) is depicted in Fig. 1. A minimal model of $3d-4p$ hybridization in Ref. [8] yields a guide to Dirac multipoles in resonant x-ray and neutron Bragg diffraction. The axial dipole is suitably small and spin-only in the model. Corresponding Dirac multipoles that contribute to resonant x-ray and neutron diffraction are found to be similar. This finding bolsters the relevance of the reported observation of Dirac multipoles in hematite by x rays [9] in a proper analysis of neutron diffraction by hematite. An important difference between amplitudes for resonant x-ray and neutron diffraction is the absence of radial integrals in the former. Notably, all radial integrals in the polar dipole displayed in Fig. 2 are of a similar size at the Bragg spot $(-7, 1, 2)_m$ where the reflection vector $\kappa \approx 5.22$ Å^{-1}.

IV. POLARIZED NEUTRON DIFFRACTION

A PND signal $\Delta = \{\mathbf{P}\cdot[\mathbf{e}\times(\langle\mathbf{Q}\rangle\times\mathbf{e})]\}$, where $\mathbf{P}$ is polarization of the primary neutrons and $\mathbf{e}$ is a unit reflection vector $\mathbf{e} = \boldsymbol{\kappa}/\kappa$. In the case of hematite phase II, the signal is in phase with nuclear diffraction by ligand ions. This is not the case for eskolaite [chromium sesquioxide (Cr_2O_3)], for example, a paradigm for the linear magnetoelectric effect (magnetic crystal class $\bar{3}'m'$). Intensity of a Bragg spot $= |\langle\mathbf{Q}\rangle - \mathbf{e}(\langle\mathbf{Q}\rangle\cdot\mathbf{e})|^2$.

Thoma *et al.* chose $\mathbf{P}$ parallel to $\mathbf{a}_h + 2\mathbf{b}_h = a(0, \sqrt{3}, 0)$ [13]. For whatever reasons, the authors do not mention the compulsory polar magnetism, or the published observation of Dirac multipoles in hematite, or the direct confirmation of neutron scattering by Dirac multipoles. Notwithstanding, Thoma *et al.* claim that the absolute direction of the DM interaction is deduced from their interpretation of neutron diffraction data on the reflection indexed $(4, -1, -1)_h \equiv (-7, 1, 2)_m$. It is a strong out-of-plane Bragg spot for which the Fe nuclear structure factor is 0. Referring to radial integrals displayed in Fig. 2, the result $\kappa = (2\pi/a\sqrt{3})[3H_o^2 + (H_o + 2K_o)^2 + 3(tL_o)^2]^{1/2}$ yields $\kappa \approx 5.22$ Å^{-1} for $(4, -1, -1)_h$.

The correct PND signal to be confronted with a Bragg diffraction pattern $\Delta = (\Delta^{(+)} + \Delta^{(-)})$ with axial and Dirac contributions labeled by our parity signature $\sigma_\pi(\pm 1)$. For axial multipoles,

$$\begin{aligned}\Delta^{(+)} = (Z^2/6)\,\{&\sin(\beta_o)\langle Q_\xi\rangle^{(+)}[k(h-k)\\ &+ 3t^2(k-l)\,(h+3l)]\\ &- \langle Q_\eta\rangle^{(+)}(1/\sqrt{3})[h(h-k) + 3t^2(h+3l)^2]\\ &- \cos(\beta_o)\langle Q_\zeta\rangle^{(+)}(t/\sqrt{3})[(1/3)h^2 + k^2 + l(h+3k)\\ &+ t^2(h+3l)^2]\}. \end{aligned} \tag{6}$$

The diffraction amplitude $\langle\mathbf{Q}\rangle = (\langle Q_\xi\rangle\boldsymbol{\xi},\ \langle Q_\eta\rangle\boldsymbol{\eta},\ \langle Q_\zeta\rangle\boldsymbol{\zeta})$. Equation (6) is a quadratic function of Miller indices and, thus, identical for (h, k, l) and $(-h, -k, -l)$. Likewise, $\Delta^{(-)}$ derived from Dirac multipoles to be considered. In Eq. (6),

$$R = [1 + 3t^2]^{1/2}, \quad Z^2[(1/3)h^2 + k^2 + t^2(h+3l)^2] = 3, \tag{7}$$

with the obtuse angle $\cos(\beta_o) = -t\sqrt{3}/R$ and $\sin(\beta_o) = (1/R)$. By way of an interesting example, the reflection vector $(2, -1, 3)_h \equiv (-3, 1, 2)_m$ is parallel to $\mathbf{a}_h$ and normal to $\mathbf{P}$. In this case, $Z^{-2} = [(4/3) + 3t^2]$ and

$$\begin{aligned}\Delta^{(+)} = -(1/2)\,\{&\sin(\beta_o)\langle Q_\xi\rangle^{(+)} + \sqrt{3}\langle Q_\eta\rangle^{(+)}\\ &+ \cos(\beta_o)\,\langle Q_\zeta\rangle^{(+)}\},\ (-3,\ 1,\ 2)_m. \end{aligned} \tag{8}$$

Evaluated at the level of dipoles,

$$\begin{aligned}\langle Q_\xi\rangle^{(+)} &\approx (3/2)[\alpha+\beta]\langle T_\xi^1\rangle,\\ \langle Q_\eta\rangle^{(+)} &\approx (3/2)[\alpha-\beta]\langle T_\eta^1\rangle,\\ \langle Q_\zeta\rangle^{(+)} &\approx (3/2)[\alpha+\beta]\langle T_\zeta^1\rangle. \end{aligned} \tag{9}$$

Higher order axial multipoles in $\langle\mathbf{Q}\rangle^{(+)}$ include a quadrupole proportional to $\langle j_2(\kappa)\rangle$ that is allowed by an admixture of manifolds in the Fe electronic ground state [15,19].

A general expression for the PND signal derived from Dirac multipoles is cumbersome, unlike the axial case Eq. (6) that is correct for all allowed multipoles. The absence of selection rules on projections in multipoles is largely responsible for cumbersome expressions. At a first level that uses anapoles $(K = 1)$,

$$\begin{aligned}\Delta^{(-)} \approx iZ/(2\sqrt{3})\,\{&\cos(\beta_o)\langle Q_\xi\rangle^{(-)}(k+3l)\\ &+ \langle Q_\eta\rangle^{(-)}t(h+3l)\\ &+ \sin(\beta_o)\,\langle Q_\zeta\rangle^{(-)}[h-k+3t^2(h+3l)]\}. \end{aligned} \tag{10}$$

In this result,

$$\begin{aligned}\langle Q_\xi\rangle^{(-)} &= (1/2)[\alpha+\beta]\,\langle d_\xi\rangle,\\ \langle Q_\eta\rangle^{(-)} &= (1/2)[\alpha-\beta]\,\langle d_\eta\rangle,\\ \langle Q_\zeta\rangle^{(-)} &= [\alpha+\beta]\,\langle d_\zeta\rangle, \end{aligned} \tag{11}$$

with $\langle \mathbf{d} \rangle$ defined in Eq. (5). Using $\sigma_\pi = -1$, the functions α and β in Eq. (2) are proportional to $i\ \sin(\varphi)$ and $i\ \sin(\varphi')$, respectively, that have opposite signs for (h, k, l) and $(-h, -k, -l)$. Beyond the approximate result Eq. (10), we have mentioned the important role of the polar spin quadrupole in an analysis of diffraction patterns for Hg1201 and YBCO, for example, and it is proportional to the radial integral $\langle h_1 \rangle$ contained in Fig. 2. The result Eq. (10) for $(-3, 1, 2)_m$ does not undergo a great simplification unlike Eq. (8).

Applications of identities $[\sin(\varphi) - \sin(\varphi')] = [\cos(\varphi) + \cos(\varphi')] = 0$ for Miller index k odd, l even, and $K = 1$ in Eqs. (9) and (11) are captured by $\langle \mathbf{Q}(C2/c) \rangle = (\langle \mathbf{Q}_\xi \rangle^{(+)}, \langle \mathbf{Q}_\eta \rangle^{(-)}, \langle \mathbf{Q}_\zeta \rangle^{(+)})$ and $\langle \mathbf{Q}(C2'/c') \rangle = (\langle \mathbf{Q}_\xi \rangle^{(-)}, \langle \mathbf{Q}_\eta \rangle^{(+)}, \langle \mathbf{Q}_\zeta \rangle^{(-)})$. These relations are particular examples of general identities valid for Miller index k odd, namely, $[\alpha \pm \beta]^{(+)} = [\alpha - (\pm)\beta]^{(-)} = 0$ with $\Phi(-1)^{K+l} = \pm 1$.

A so-called spin-flip intensity is the fraction of neutrons that participate in events that change (flip) the neutron spin orientation [17,18]. For a collinear magnetic motif and complete polarization, $P^2 = 1$, the fraction,

$$\mathrm{SF} = \{|\langle \mathbf{Q}_\perp \rangle|^2 - |\mathbf{P} \cdot \langle \mathbf{Q}_\perp \rangle|^2\}, \tag{12}$$

with $\langle \mathbf{Q}_\perp \rangle = [\mathbf{e} \times (\langle \mathbf{Q} \rangle \times \mathbf{e})]$ is a measure of the magnetic content of a Bragg spot. For the special case $\mathbf{P} \cdot \mathbf{e} = 0$, Eq. (12) reduces to $\mathrm{SF} = \{|\langle \mathbf{Q} \rangle|^2 - |\mathbf{e} \cdot \langle \mathbf{Q} \rangle|^2 - |\mathbf{P} \cdot \langle \mathbf{Q} \rangle|^2\}$. Applied to orthogonal $\mathbf{e} \propto \mathbf{a}_h$ and $\mathbf{P} \propto \mathbf{b}_h^*$, the polarization used in Ref. [13], the spin-flip intensity measures the component of $\langle \mathbf{Q} \rangle = (\langle \mathbf{Q} \rangle^{(+)} + \langle \mathbf{Q} \rangle^{(-)})$ parallel to the crystal $\mathbf{c}$ axis, i.e., $\mathrm{SF} = |\cos(\beta_o)\langle Q_\xi \rangle - \sin(\beta_o)\langle Q_\zeta \rangle|^2$. In consequence, SF at the Bragg spot $(-3, 1, 2)_m$ measures diffraction by axial dipoles in $C2/c$ and anapoles in $C2'/c'$, respectively.

V. DISCUSSION

In summary, our calculations of neutron diffraction amplitudes for room-temperature hematite (α-Fe_2O_3, phase II) demonstrate a wealth of information in a Bragg diffraction pattern. Calculations encompass two candidate magnetic structures and axial and polar (Dirac) multipoles. The latter exist in phase II according to published resonant x-ray diffraction data [9], and anapoles are known to deflect neutrons [10]. The open question posed by the magnetic structure is not adequately addressed, and Dirac multipoles find no place in a recent account of a polarized neutron diffraction study of hematite [13].

In more detail, axial magnetic signatures to be confronted with a measurement of the Bragg spot $(-7, 1, 2)_m$ in Ref. [13] are shown by us to be $\Delta^{(+)} \propto [-\langle Q_\xi \rangle^{(+)} + 0.74\langle Q_\zeta \rangle^{(+)}]$ or $\Delta^{(+)} \propto \langle Q_\eta \rangle^{(+)}$ for candidate magnetic space groups $C2/c$ and $C2'/c'$, respectively. Here, $\langle \mathbf{Q} \rangle^{(+)}$ is the axial neutron scattering amplitude and $(\boldsymbol{\xi}, \boldsymbol{\eta}, \boldsymbol{\zeta})$ Cartesian vectors in the monoclinic magnetic structure with unique axis η. The mentioned expressions are correct at the level of dipoles ($K = 1$), results in Eq. (9) apply, and $\langle \mathbf{Q} \rangle^{(+)}$ is proportional to the axial magnetic moment $\langle 2\mathbf{S} + \mathbf{L} \rangle$ in the forward direction of scattering. With regard to higher order axial multipoles, quadrupoles might be influential for two reasons. First, such quadrupoles are proportional to the radial integral $\langle j_2(\kappa) \rangle$. Reference to results for radial integrals in Fig. 2 shows that $\langle j_0(\kappa) \rangle$ and $\langle j_2(\kappa) \rangle$ that together make up $\langle \mathbf{Q} \rangle^{(+)}$ are almost equal in magnitude at the Bragg spot $(-7, 1, 2)_m$ where the reflection vector $\kappa \approx 5.22$ Å^{-1}. Secondly, the absence of symmetry of Fe sites allows for significant mixing of atomic manifolds and an axial quadrupole, or an inextricable knot of spin and space using the spin anapole represented by the operator equivalent $\mathbf{n}(\mathbf{S} \times \mathbf{n})$ [15,19]. Equations (10) and (11) for anapoles reveal PND signals $\Delta^{(-)} \propto [\langle Q_\xi \rangle^{(-)} + 1.89\langle Q_\zeta \rangle^{(-)}]$ and $\Delta^{(-)} \propto \langle Q_\eta \rangle^{(-)}$ for space groups $C2'/c'$ and $C2/c$, respectively, for the Bragg spot $(-7, 1, 2)_m$.

With future neutron diffraction experiments on room-temperature hematite in mind, we report the spin-flip intensity for the convenient Bragg spot $(-3, 1, 2)_m$, $\kappa \approx 2.85$ Å^{-1}. The ratio measures the magnetic content of a Bragg spot, and the technique has been used extensively to study ceramic superconductors, e.g., Hg1201 and YBCO [20]. Axial dipoles in $C2/c$ and anapoles in $C2'/c'$ are detected, respectively, for the chosen conditions of orthogonal neutron polarization and reflection vector.

ACKNOWLEDGMENTS

D. D. Khalyavin provided details of the magnetic space groups. V. Scagnoli is the author of Fig. 1. G. van der Laan calculated radial integrals that appear in Fig. 2 and created the figure.

[1] P. J. Brown and J. B. Forsyth, J. Phys.: C Solid State Phys. **14**, 5171 (1981).
[2] P. J. Brown, Phys. B (Amsterdam, Neth.) **192**, 14 (1993).
[3] Q. Zhang, J. Liang, K. Bi, L. Zhao, H. Bai, Q. Cui, H. A. Zhou, H. Bai, H. Feng, W. Song *et al.*, Phys. Rev. Lett. **128**, 167202 (2022).
[4] M. Catti, G. Valerio, and R. Dovesi, Phys. Rev. B **51**, 7441 (1995); A. H. Morrish, *Canted Antiferromagnetism: Hematite* (World Scientific, Singapore, 1994); *International Tables for Crystallography*, Vol. D, Section 1.5.3, 2013.
[5] I. Dzyaloshinskii, J. Phys. Chem. Solids **4**, 241 (1958).
[6] T. Moriya, Phys. Rev. **120**, 91 (1960).
[7] K. A. Milton, Rep. Prog. Phys. **69**, 1637 (2006).
[8] J. Fernández-Rodríguez, V. Scagnoli, C. Mazzoli, F. Fabrizi, S. W. Lovesey, J. A. Blanco, D. S. Sivia, K. S. Knight, F. de Bergevin, and L. Paolasini, Phys. Rev. B **81**, 085107 (2010).
[9] S. W. Lovesey, A. Rodríguez-Fernández, and J. A. Blanco, Phys. Rev. B **83**, 054427 (2011); A. Rodríguez-Fernández, J. A. Blanco, S. W. Lovesey, V. Scagnoli, U. Staub, H. C. Walker, D. K. Shukla, and J. Strempfer, *ibid.* **88**, 094437 (2013).
[10] S. W. Lovesey, T. Chatterji, A. Stunault, D. D. Khalyavin, and G. van der Laan, Phys. Rev. Lett. **122**, 047203 (2019).
[11] We use the BNS setting of magnetic space groups; see Bilbao Crystallographic server, http://www.cryst.ehu.es.

[12] R. Przeniosło, I. Sosnowska, M. Stękiel, D. Wardecki, A. Fitch, and J. B. Jasiński, Phys. B (Amsterdam, Neth.) **449**, 72 (2014).
[13] H. Thoma, V. Hutanu, H. Deng, V. E. Dmitrienko, P. J. Brown, A. Gukasov, G. Roth, and M. Angst, Phys. Rev. X **11**, 011060 (2021).
[14] S. W. Lovesey, E. Balcar, K. S. Knight, and J. Fernández Rodríguez, Phys. Rep. **411**, 233 (2005).
[15] S. W. Lovesey, Phys. Scr. **90**, 108011 (2015).
[16] R. D. Cowan, J. Opt. Soc. Am. **58**, 808 (1968).
[17] S. W. Lovesey, D. D. Khalyavin, and U. Staub, J. Phys.: Condens. Matter **27**, 292201 (2015).
[18] S. W. Lovesey and D. D. Khalyavin, J. Phys.: Condens. Matter **27**, 495601 (2015).
[19] D. D. Khalyavin and S. W. Lovesey, Phys. Rev. B **100**, 224415 (2019).
[20] P. Bourges, D. Bounoua, and Y. Sidis, Comptes Rendus Physique **22**, 1 (2021).